Available online at www.sciencedirect.com

SciVerse ScienceDirect

Ceramics International 39 (2013) 6727–6734

CERAMICS INTERNATIONAL

www.elsevier.com/locate/ceramint

Inherent defects in sol-precipitation/hydrothermally derived $SrTiO_3$ nanopowders

Tina Šetinc[a,*], Matjaž Spreitzer[a], Damjan Vengust[a], Ivan Jerman[b], Danilo Suvorov[a]

[a]*Advanced Materials Department, Jožef Stefan Institute, Ljubljana, Slovenia*
[b]*Laboratory for the Spectroscopy of Materials, National Institute of Chemistry, Ljubljana, Slovenia*

Received 24 January 2013; received in revised form 30 January 2013; accepted 31 January 2013
Available online 8 February 2013

Abstract

We have investigated sol-precipitation, coupled with a hydrothermal treatment, as a common solution-based method for the preparation of $SrTiO_3$ nanostructured powders. XRD, FTIR, TG/EGA, Raman and TEM were employed for a detailed structural characterization of the sol-precipitates in comparison with subsequently hydrothermally or thermally post-annealed samples. The sol-precipitates exhibited a pseudo-cubic symmetry and adopted the morphology of the hydrolyzed Ti-precursor. The structural distortions were attributed to un-removed OH^- groups and A-site vacancies, arising in the crystal lattice, as a result of a low-temperature diffusion-controlled reaction. Furthermore, we demonstrated that the microstructural characteristics of sol-precipitates are directly responsible for the formation of extended defects, i.e., nanocavities, within the single-crystalline particles, appearing independently of the selected post-annealing treatment, i.e., hydrothermal or thermal. The study revealed that local distortions and peculiarities on the microscale, introduced by sol-precipitation, were not completely restored under vigorous hydrothermal conditions, but rather provoked the formation of new microstructural defects with an additional treatment.

Keywords: A. Powders: chemical preparation; B. Defects; $SrTiO_3$; Microstructure; Sol-precipitation; Hydrothermal synthesis

1. Introduction

$SrTiO_3$ (abbreviated as ST) is one of the most studied perovskites, noted for its quantum paraelectric behavior [1] and mixed ionic-covalent bonding, which give rise to a unique electronic structure and intriguing properties for microwave electronic applications [2]. At room temperature, ST assumes a prototypic cubic perovskite structure, whereas at cryogenic temperatures, an antiferrodistortive phase transition to a tetragonal structure (space group *I4/mcm*) occurs [1]. However, studies also indicate stoichiometry-related difficulties, giving rise to a locally non-centrosymmetric structure that results in an anomalous dielectric or ferroelectric response [3,4]. In addition to the structural defects, the behavior of ST is also influenced by microstructural properties, particularly below a certain size of the particles. Accordingly, the structural and microstructural defects remain of key importance for the functional performance of ST, and defects should be investigated within the context of the synthesis technique applied.

In the past, the processing of ST powders was focused on the wet chemical methods and accordingly numerous different approaches have been utilized for the preparation of nanostructured ST powders, i.e., molten salt synthesis [5], microemulsion-mediated synthesis [6], Pechini and related methods [7], thermal decomposition of suitable precursors [8], decomposition of bimetallic alkoxide precursors [9], hydrothermal [10], and precipitation from a precursor solution or gel suspension in a strong alkaline environment [11].

Recently, Calderone et al. [12] demonstrated the effectiveness of using sol-precipitation from a titanium hydroxide gel suspension, which enabled them to prepare defective single-crystalline ST particles with a tailored size (80–1400 nm) by careful control of the synthesis conditions. Herein, the oriented aggregation or epitaxial self-assembly of small nanocrystallites was proposed as the

*Corresponding author. Tel.: +386 1 477 3991.
E-mail addresses: tina.setinc@ijs.si, tina.setinc@gmail.com (T. Šetinc).

0272-8842/$ - see front matter © 2013 Elsevier Ltd and Techna Group S.r.l. All rights reserved.
http://dx.doi.org/10.1016/j.ceramint.2013.01.115

growth mechanism that yielded porous monocrystallites. In addition, the sol-precipitation was coupled with a hydrothermal treatment [13–15], as a two-step synthesis procedure. Although different modifications of the latter synthesis were employed, all studies collectively reported the formation of cubic-shaped crystallites with distinct circular- and square-shaped anomalies being present. Detailed TEM investigations excluded the possibility that these were surface-related defects, whereas thickness mapping has revealed the depletion of material across the defective regions, which suggested the presence of nanocavities within the crystallites [13]. Although these anomalous features were collectively observed for hydrothermally post-treated sol-precipitates, the cause of the formation was neither suggested nor explored.

Accordingly, we have performed a detailed structural and microstructural investigation of ST powders derived from sol-precipitation in comparison to a hydrothermally post-treated sample. To estimate the actual contribution of the hydrothermal conditions, precipitated powders were also thermally annealed, and an investigation from the microstructural point of view was performed. Sol-precipitation, as a low-temperature ambient-pressure synthesis technique, requires reactive precursors for the formation of the perovskite phase. Therefore, chloride-based precursors are commonly used. However, to avoid any possible contamination with Cl^- ions, titanium alkoxide and strontium hydroxide were selected as the initial reagent.

2. Experimental procedure

The experimental procedure was performed as illustrated in the flow chart (Fig. 1). The sol-precipitation was carried out by dissolving $Sr(OH)_2 \ldots 8H_2O$ (Alfa Aesar, 99%) in 1 M acetic acid (pH ~ 2.5) at 95 °C, yielding a clear Sr-precursor solution. With the addition of titanium (IV) isopropoxide (Alfa Aesar, 97+%) the final solution of 0.1 M concentration and an equimolar Sr/Ti ratio was obtained. The precipitation of $SrTiO_3$ was induced by slowly adding sodium hydroxide pellets (Applichem, pellets, min 99%) to the precursor solution, attaining a NaOH concentration of 3 M (pH > 13). After precipitation the reaction suspension was stirred for 0.5 h at 95 °C. The resulting precipitates were subsequently collected and washed during the centrifugation and water re-dispersion cycle, repeated three times to remove the remaining species. The prepared sol-precipitate (abbreviated as ST–SP) powders were air-dried at 95 °C overnight prior to their characterization. The hydrothermally derived samples were prepared using an identical sol-precipitation procedure to that described above, only in this case the suspension obtained after the precipitation was directly transferred into a 100 ml Teflon-lined autoclave with a 30% filling capacity and heated to 240 °C for 12 h. The autoclave was subsequently allowed to cool to room temperature. The hydrothermally treated precipitates were afterwards washed and dried using the same procedure as employed for the ST–SP product. In this way hydrothermally derived powders were obtained (abbreviated as ST–HT).

In addition, ST powders were also prepared by solid-state reaction (abbreviated as ST–SS) for the reference structural investigations. Stoichiometric amounts of TiO_2 (rutile, 99.99%, Alfa Aesar) and $SrCO_3$ (99.99%, Alfa Aesar) powders were dried at 200 °C for 2 h prior to their homogenization in absolute ethanol. The reactant powders were pressed into pellets and pre-reacted at 1000 °C for 10 h. The pellets were subsequently crushed, ball milled and then calcined at 1250 °C for 10 h. This procedure was repeated, with the final calcination being conducted at 1400 °C for 10 h.

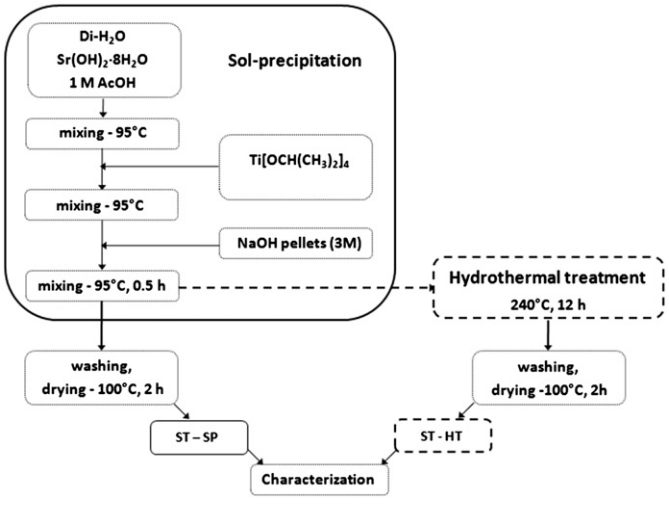

Fig. 1. Synthesis procedure employed for the preparation of ST sol-precipitates and hydrothermally derived ST powders.

2.1. Measurements

The X-ray powder-diffraction patterns were collected in the 2-theta range 20°–80° using a PANalytical X'Pert PRO (radiation wavelength CuKa = 1.5406 Å) with a Johansson monochromator. Ordinarily, XRD diffractograms were recorded with a step of 0.017° and a counting time of 1 s, except for the precise diffractograms in the 67–69° 2-theta range, recorded with a step of 0.008° and a counting time of 10 s. For the Fourier-transform infrared spectroscopy (FTIR) measurements, the as-prepared powders were triturated with KBr and pressed into pellets. The FTIR spectra of the ST powders were recorded with a Bruker IFS 66/S in the wavenumber region from 400 to 4000 cm^{-1} with a resolution of 4 cm^{-1} and with 64 scans for each sample. Simultaneous thermogravimetric (TG) and evolved-gas analysis (EGA) were conducted in air from 30 to 1000 °C with a heating rate of 5 °C/min using a Jupiter 449&403C Aë]oloss, Netzch. The Raman spectra were recorded on a Raman Witec alpha 300 spectrometer employing a 532 nm green laser. The microstructural characterization was performed with a transmission electron microscope (TEM, Jeol, JEM-2100).

3. Results and discussion

3.1. XRD

In Fig. 2(a), XRD patterns of the as-prepared, precipitated SP, hydrothermally annealed HT versus bulk SS ceramics are presented. The main diffraction peaks of all the samples correspond to the perovskite structure; however, some less intense additional reflections were noticed in the diffractograms of the SP and HT samples, indicating a minor content of impurity phases (Fig. 2b). The broad secondary peaks in the diffraction pattern of the SP powders corresponded to $SrCO_3$ (JCPDS No. 84-1778) and the pseudobrookite Ti_3O_5 polytype (JCPDS No.72-2101). The HT sample exhibited several sharp diffraction peaks of low intensity that were assigned to sodium acetate hydrate (JCPDS No. 28-1303), presumably crystallizing from the un-removed precursor species upon cooling after the reaction was terminated. As with the ST phase in the SP sample, a pseudo-cubic symmetry was observed, whereas only the pattern of the SS sample is totally consistent with the *Pm3m* space group (JCPDS No. 86-0176). The estimated FWHM (Full Width at Half Maximum) values are 0.253°, 0.164° and 0.067°, for the SP, HT and SS powders, respectively. The corresponding increase in FWHM values, being crystallite-size or microstrain related, is accompanied by a proportional shift of the peaks toward lower 2-theta values, as is evident from Fig. 2(c). The lattice expansion can be related to the non-stoichiometry on the Sr^{2+} sites, as previously described by Brooks et al. [16]. In our experiment, vacancies on the A-sites might arise due to the low-temperature diffusion-controlled reaction between the Sr^{2+} ions and the $[Ti(OH)_6]^{2-}$, i.e., a hydrolyzed titanium gel precursor. Considering that crystallization of the ST phase also requires the elimination of OH^- groups from the titanium precursor [17], an incomplete transformation might also result in the residual OH^- within the perovskite structure. According to Beran et al. [18], a structural model for OH^- groups, incorporated into the perovskite crystal lattice, assumes the formation of A-site vacancies, which compensate for the charge imbalance and also for the strain and stress effects. Thus, the expansion of the unit cell or distortions in the crystal symmetry might arise due to the presence of hydroxyl groups, which at the same time oppose the occupation of A-sites. Nevertheless, the distortions observed for the SP powders are reduced by a further hydrothermal treatment, as determined from the corresponding XRD patterns of the HT sample. Indications of hydroxyl groups and other precursor-related species for the SP and HT powders were further investigated by means of FTIR analyses.

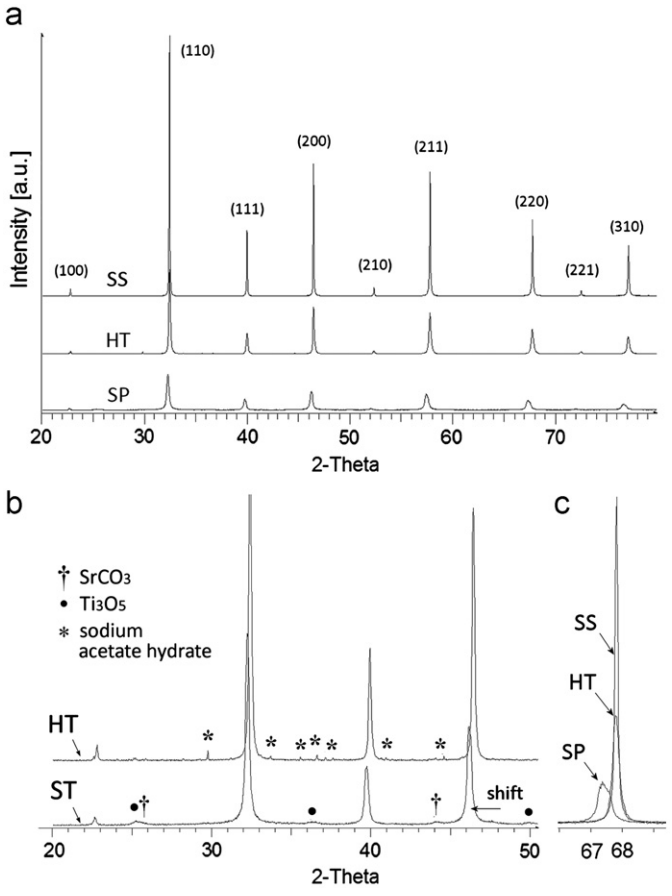

Fig. 2. (a) XRD diffraction patterns of sol-precipitated (SP), hydrothermally post-treated precipitates (HT), and bulk ceramics, prepared by solid-state reaction (SS). (b) Diffractograms of SP and HT sample with arrows denoting traces of secondary phases. (c) High-precision scans of (220) reflections, recorded in the 2-theta 67–69° range of SP, HT, and SS powders.

3.2. Fourier-transform infrared spectroscopy

The FTIR spectra of the SP and HT samples are shown in Fig. 3. Within the measured range, several distinct absorption bands were observed. The broad, low-intensity absorption band in the range 3400–3600 cm^{-1} is caused by

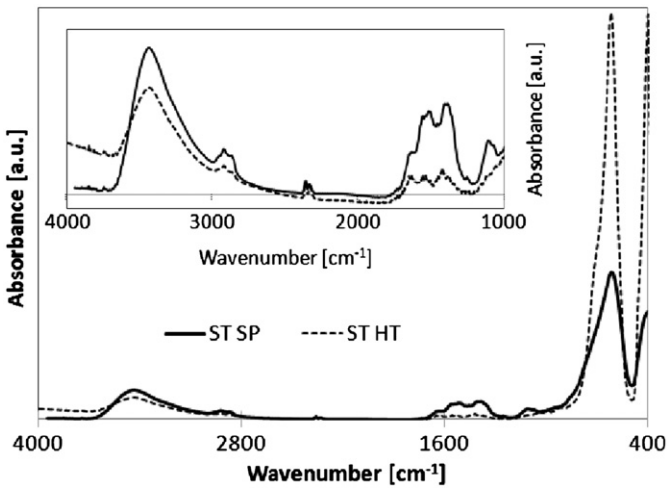

Fig. 3. FT-IR results of SP and HT samples. The inset shows more precisely the low-intensity absorption bands, related to vibrations of the precursor groups.

vibrations of the O–H bonds arising from either the surface hydroxyl groups or the O–H groups from the physically adsorbed water [19]. The presence of O–H groups is to some extent characteristic of the powders obtained by a reaction in an alkaline aqueous solution and/or hydrothermally synthesized powders. The absorption in the range 2850–3000 cm^{-1} is due to C–H sp^3 stretching and can be ascribed to the vibrations of the alkyl groups of the titanium precursor, acetic acid, and the corresponding derivatives. The small, double-maximum peak at ~2350 cm^{-1} is due to the asymmetric stretching of the CO_2, originating from the decomposition of titanium isopropoxide [20]. The two absorption peaks near 1400 and 1520 cm^{-1} correspond to the symmetric and asymmetric stretching vibrations of the carboxylate groups [20], i.e., from the acetate ligands of acetic acid. The absorption between 1000 and 1100 cm^{-1} is due to the stretching vibration of the C–O alcohol groups, corresponding to the titanium precursor. Furthermore, the IR spectrum exhibits two strong absorption bands, located at about 400 and 620 cm^{-1}, which are attributed to the vibrations of the Ti–O bonds within the TiO_6 octahedron, bending at lower-frequency and stretching at higher-frequency [21], respectively. The latter peaks are characteristic for the perovskite structure and, as observed, the corresponding absorbance is significantly higher for the HT powders. The results suggest that the sol-precipitation results in crystalline ST powders; however, the pronounced absorption bands associated with the precursor species for the SP sample are indicative of an incomplete reaction toward the perovskite structure. Thus, the subsequent hydrothermal treatment promoted the crystallization process, as determined from the FTIR and XRD results. The SP and HT powders were subjected to TG and EGA analyses to acquire supplemental data regarding the possible elimination of H_2O groups and the decomposition behavior of the unreacted species, as identified by FTIR spectroscopy.

3.3. TG and EGA analysis

Thermogravimetric curves of the as-prepared ST powders are shown in Fig. 4. The estimated weight losses of the sol-precipitate and the hydrothermally derived sample are 9.7% and 2.6%. In the case of the SP powders, the first contribution to the weight loss of ~3.6% between room temperature and 200 °C is due to the elimination of water, i.e., a dehydration process. Later, a gradual decrease in the weight between 200 °C and 600 °C is related to the emission of CO_2 and thus ascribed to the pyrolysis of the carboxyl precursor groups (in accordance with the FTIR results) with an overall contribution of ~3.0% to the total weight loss. Between 700 °C and 900 °C, a final weight loss of ~3.1%, also resulting from CO_2 emission, is determined and ascribed to the decomposition of $SrCO_3$, based on the corresponding thermal analysis data [22]. The latter arises due to the reaction of atmospheric CO_2 with Sr^{2+} ions from the system. According to previous studies, the residual $SrCO_3$ can exist in the form of separate particles or on the surface of the ST grains [23]. With respect to the HT sample, a total weight loss of 2.6% is determined. The first contribution of ~0.4% up to 200 °C is related to the elimination of H_2O, the dehydration process. Furthermore, an explicit step in the weight loss of 1.4% is perceived between 250 °C and 500 °C, originating from two contributions, i.e., the CO_2 emission and the evaporation of H_2O. As determined from the mass spectra, the two peaks coincide. Within the referred to temperature zone, the water elimination might be attributed to the removal of OH^- groups, i.e., the dehydroxylation of the HT nanocrystals [24]. The incorporation of hydroxyl groups in the regular perovskite lattice has been previously addressed [25–30], and the latter is closely associated with nanopowders derived from an alkaline-based aqueous medium. However, the bounding site of the OH^- groups, i.e., being bulk or surface-related phenomena, remains uncertain here. Bulk incorporation, nevertheless, results in a defect structure and consequently a distorted local symmetry. To verify the possible structural distortions arising for the prepared ST powders, Raman spectroscopy was employed.

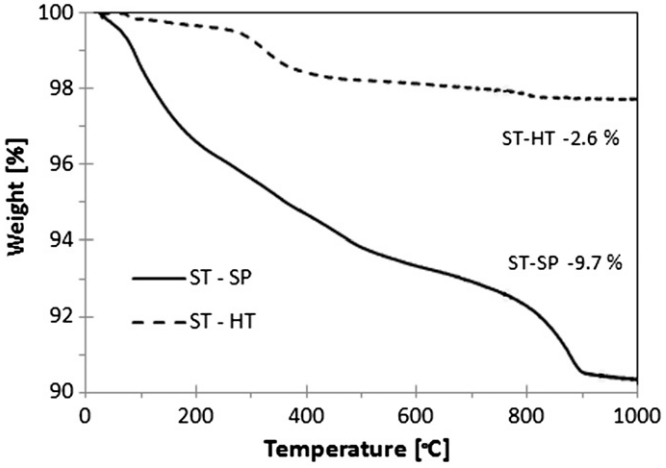

Fig. 4. TG curves of SP and HT sample.

3.4. Raman spectroscopy

Under ambient conditions, ST exhibits an ideal cubic structure with the *Pm3m* space group. This means that no first-order Raman scattering is allowed, based on symmetry considerations, and the spectrum is expected to be dominated by second-order activity [31]. As reported previously [32], the second-order dynamics is observed in two broad bands centered in the 200–500 $cm^{-1}$and 600–800 cm^{-1} regions of the spectrum; therefore, activity in the corresponding regions will not be further specifically addressed. For the low-temperature ST tetragonal structure of the *I4/mcm* space group, seven Raman active modes including two degenerate $\{E_g, B_{1g}\}$ and a B_{2g} mode were reported [31,32], with the corresponding bands observed in the ranges 140–150 cm^{-1}, 440–460 cm^{-1}, and 220–260 cm^{-1}. However, a strong peak at ~146 cm^{-1}, previously assigned by Banerjee et al. [33] to the E_g mode, was also related to the $SrCO_3$ content in the

specimen; therefore, the corresponding scattering will not be taken into consideration. Fig. 5 represents the Raman spectra of the SP and HT samples in relation to the scattering behavior of the SS bulk ceramic. Second-order activity is clearly observed for the ST–SS sample, whereas the SP and HT samples exhibited somewhat different behavior. The corresponding Raman spectra were differentiated in terms of the appearance of additional peaks outside the expected second-order scattering regions. The sol-precipitates exhibited two additional peaks at 176 and 543 cm^{-1}, whereas the HT sample showed several peaks of low intensity. However, the following peaks at 176, 543, and 796 cm^{-1} are sufficiently explicit to consider. The recorded Raman shifts at 176, 543, and 796 cm^{-1} agree well with the frequencies of the TO_2, TO_4, and LO_4 [31,32], respectively, and are indicative of the first-order scattering behavior. Previously, this phenomenon was collectively observed for ST nm- and μm-sized powders [13,33], thin films [34], as well as at fine- and coarse-grained bulk ceramics [3]. Distortions from the ideal cubic structure have been attributed to non-stoichiometry, such as impurities [33] and oxygen vacancies [3,13,33]. The latter compositional fluctuations distort the long-range ordering and cubic symmetry. Thus, the ambient IR active polar modes demonstrate the loss of the local inversion symmetry for the as-prepared SP as well as HT powders.

3.5. TEM characterization

TEM investigation of the SP powders (Fig. 6) revealed less-defined or even cloddy-like particles that appear as aggregates of a few-nm-sized crystallites. However, the HRTEM imaging of a single aggregate-like particle (Fig. 6a) clearly shows the parallelism of the lattice fringes throughout the whole crystal with a spacing of 0.28 nm, corresponding to the {110} planes of the ST. Nevertheless, the translucent regions suggest that such crystals contain some inner voids or pores, as previously reported by Calderone [12] and Wang [35]. For the adopted morphology of the SP sample, the hydrolyzation of titanium isopropoxide into a gel precursor was considered. Repeating the identical sol-precipitation procedure, now in the absence of a strontium precursor, yielded titanium precipitates (shown in Fig. 7b) that reflected the exact microstructural characteristics, as observed for the SP powders (Fig. 7a). These results indicate that the formation mechanism, which can be adopted for the given synthesis procedure, involves the diffusion of Sr^{2+} ions into the amorphous (according to XRD, not shown here) hydrolyzed titanium gel precursor, from which the perovskite phase crystallizes, when properly alkaline conditions (pH > 13) are attained by the addition of NaOH into the stock solution. The proposed mechanism explains the morphological properties of the SP sample as well as the results from the XRD, TG and FTIR analyses, and is in agreement with the predictions of Kao and Yang [36]. The microstructural diversity of the precipitates

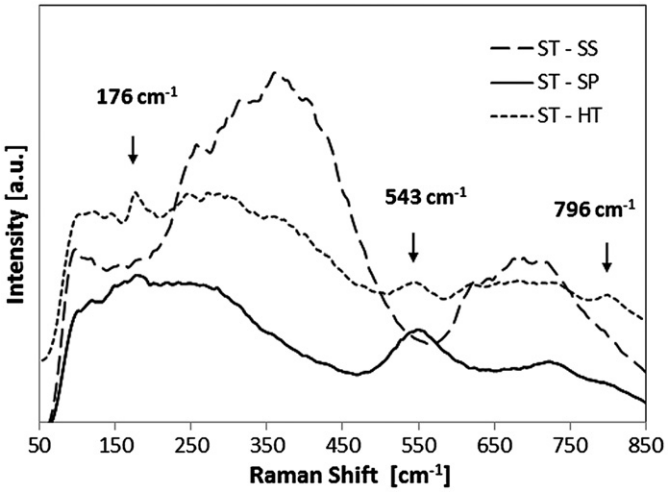

Fig. 5. Raman spectra recorded at ambient conditions of SP and HT powders, in comparison to scattering behavior of the bulk ST ceramic (SS).

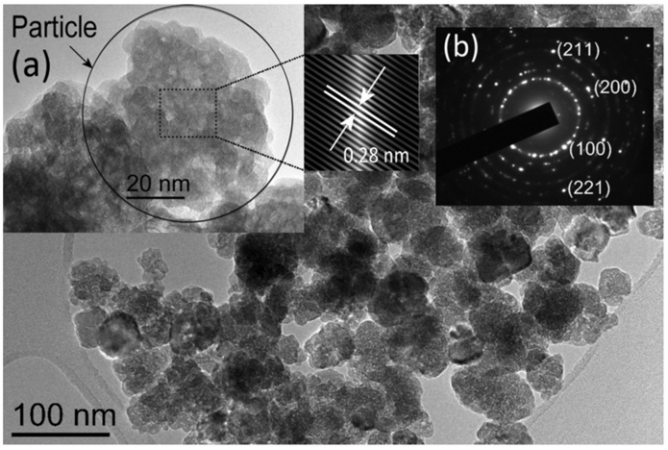

Fig. 6. Microstructure of the sol-precipitated SP sample. Inset (a) denotes a single aggregate-like particle with the corresponding fringe spacing of 0.28 nm and (b) SAED polycrystalline diffraction pattern.

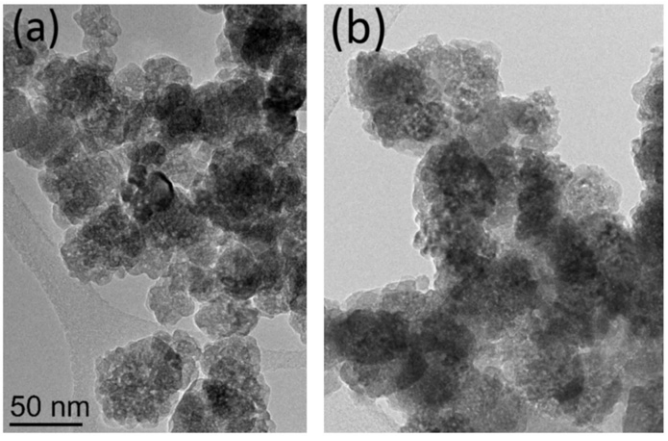

Fig. 7. Microstructural characteristics of (a) SP powders, in relation to (b) pure titanium-based precipitates.

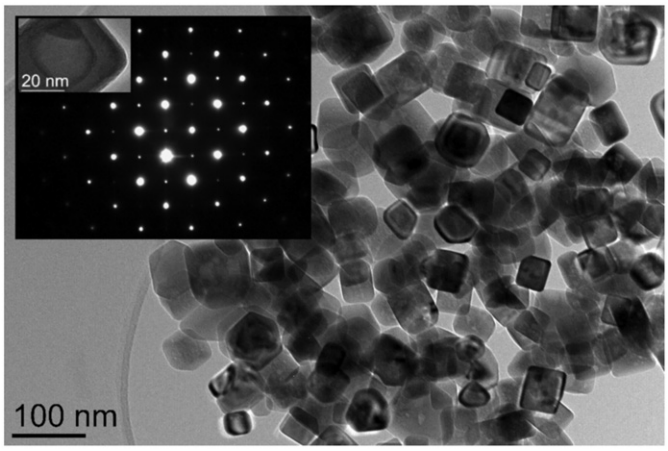

Fig. 8. TEM micrograph of HT nanoparticles. Inset on the left shows single-crystalline electron diffraction of nanoparticle along the ⟨100⟩ zone axis.

thus originates from poor control of the hydrolyzation process itself.

By further exposing the SP powders to the hydrothermal conditions, a transformation toward predominately cubic-like single-crystalline nanoparticles with well-defined facets was observed and shown in Fig. 8. The HT nanopowders exhibited some distinct features. The first types are presumably surface-related defects, which appear in the form of oriented cubic-like features (with truncated or rounded edges), perfectly aligned with the crystallite itself, appearing without interrupting the crystal's lattice fringes (Fig. 9a). Similar observations were reported by Balaya et al. [37] Also observed (for the electron beam) are highly translucent circular- or square-shaped features within the crystallites, shown in Fig. 9(b). Previous investigations [13] demonstrated that these were not surface-related phenomena but actually nanocavities within the single-crystalline particles. However, to the best of our knowledge, no explanation for, or assumption about, their occurrence has been reported in the literature. In addition to sole hydrothermal conditions, the peculiar microstructure of the SP sample, as a precursor source, is another important parameter that can be the origin of extended defects arising from a subsequent treatment. For verification of the latter, the SP powders were alternatively thermally annealed, i.e., heat treated at 900 °C for 2 h. As presented in Fig. 10, thermally annealed SP powders are from the aspect of size, shape and defects, almost identical to the HT sample. Accordingly, we have demonstrated that the defects are not conditioned by the choice of post-annealing process, but rather invoked by the microstructural characteristics of the SP sample. The unfilled regions within the SP particles can act as trapping sites for water or precursor species that remain captured or locally hinder the crystallization process during the hydrothermal post treatment. Accordingly, the HT sample results in particles that exhibit distinct inner defects, as perceived from the TEM, and are accompanied by the elimination of bulk-bounded H_2O (or CO_2 in the case of precursor species), supported by a TG/EGA analysis. It is worth noting that the inherent defects appear to be fairly stable, since no change regarding their size, distribution and shape is observable, either by repeating and/or prolonging the thermal or hydrothermal treatment of the SP powders.

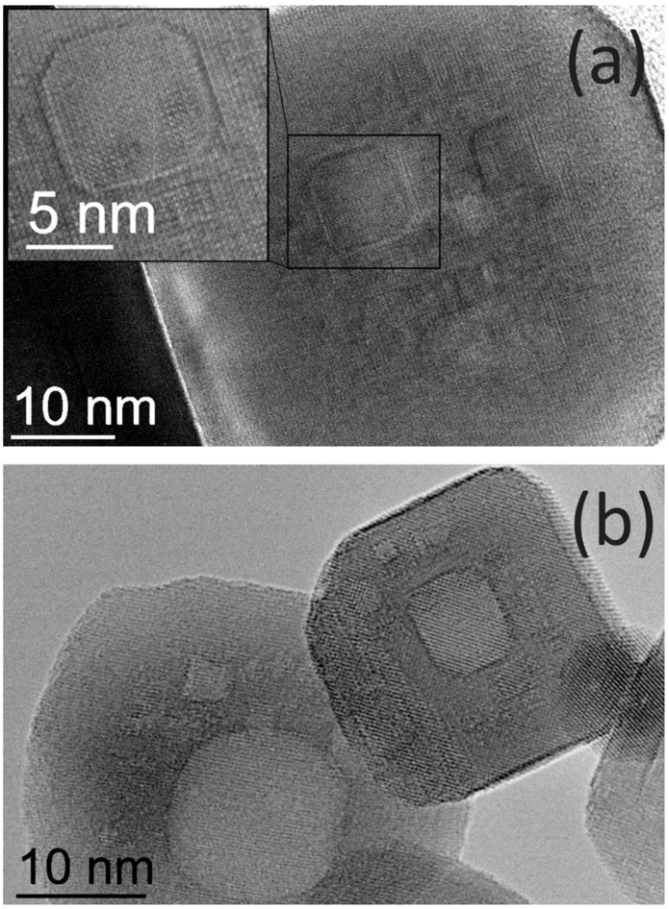

Fig. 9. TEM imaging of microstructural peculiarities, observed for HT sample, i.e., surface-related cubic features (a) and (for electron beam) translucent nanocavities (b).

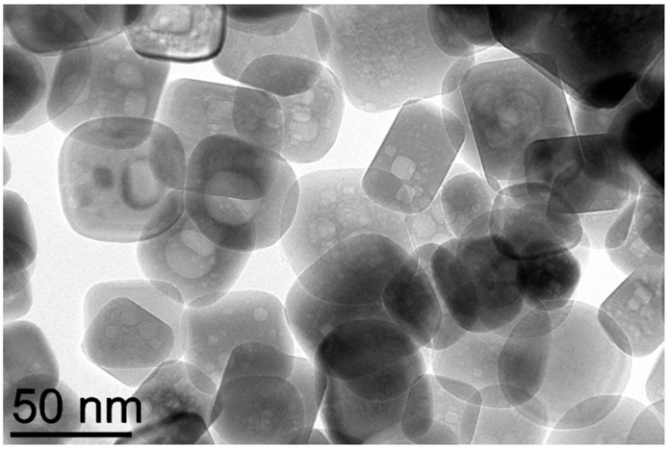

Fig. 10. ST nanoparticles obtained by thermal annealing of precipitated SP powders at 900 °C for 2 h.

4. Conclusions

Sol-precipitation-derived SP powders exhibit a highly distorted cubic symmetry that was ascribed to their non-stoichiometry, i.e., OH^- groups and vacancies on the Sr^{2+} sites. The microstructure was adopted from the hydrolyzed titanium precursor. Thus, we confirmed that the SP powders form by the diffusion of Sr ions into the hydrolyzed titanium precursor network, followed by a crystallization towards perovskite by water elimination under properly alkaline conditions. Detailed XRD, FTIR, TG/EGA and Raman analyses indicate that distortions arise due to the low-temperature, alkaline environment of the crystallization that limits the diffusion of Sr ions and hinders the elimination of residual OH^- groups, respectively.

A subsequent hydrothermal treatment improves the crystallinity of the powders, but the local disorder was still present (Raman). The hydrothermal treatment changes the morphology of the powders toward cubic-shaped single-crystalline particles that exhibited distinct surface features and nanocavities within. However, the same microstructural characteristics were also observed for a thermally annealed SP sample. Thus, we demonstrated that the latter defects are not conditioned by the post-annealing procedure, but rather grounded by the microstructural peculiarities of the precipitated SP sample. The microstructural faults remain stable after further prolongation or repetition of the hydrothermal or thermal annealing procedure.

References

[1] K.A. Müller, H. Burkard, $SrTiO_3$: an intrinsic quantum paraelectric below 4 K, Physical Review B 19 (1979) 3593–3602.

[2] A.K. Tagantsev, V.O. Sherman, K.F. Astafiev, J. Venkatesh, N. Setter, Ferroelectric materials for microwave tunable applications, Journal of Electroceramics 11 (2003) 5–66.

[3] J. Petzelt, T. Ostapchuk, I. Gregora, I. Rychetský, S. Hoffmann-Eifert, A.V. Pronin, Y. Yuzyuk, B.P. Gorshunov, S. Kamba, V. Bovtun, J. Pokorný, M. Savinov, V. Porokhonskyy, D. Rafaja, P. Vaněk, A. Almeida, M.R. Chaves, A.A. Volkov, M. Dressel, R. Waser, Dielectric, infrared, and Raman response of undoped $SrTiO_3$ ceramics: evidence of polar grain boundaries, Physical Review B 64 (2001) 184111 10.

[4] D.A. Tenne, A.K. Farrar, C.M. Brooks, T. Heeg, J. Schubert, H.W. Jang, C.W. Bark, C.M. Folkman, C.B. Eom, D.G. Schlom, Ferroelectricity in nonstoichiometric $SrTiO_3$ films studied by ultraviolet Raman spectroscopy, Applied Physics Letters 97 (2010) 142901–142903.

[5] M.E. Ebrahimi, M. Allahverdi, A. Safari, Synthesis of high aspect ratio platelet $SrTiO_3$, Journal of the American Ceramic Society 88 (2005) 2129–2132.

[6] Y.F. Li, Q.Y. Lai, Q.Y., Study on synthesis of nano-crystalline $SrTiO_3$ by the inverse micell microemulsion method, Chinese Journal of Inorganic Chemistry 21 (2005) 915–918.

[7] M. Kakihana, T. Okubo, M. Arima, Y. Nakamura, M. Yashima, M. Yoshimura, Polymerized complex route to the synthesis of pure $SrTiO_3$ at reduced temperatures: implication for formation of Sr–Ti heterometallic citric acid complex, Journal of Sol–Gel Science and Technology 12 (1998) 95–109.

[8] I.W. Lenggoro, C. Panatarani, K. Okuyama, One-step synthesis and photoluminescence of doped strontium titanate particles with controlled morphology, Materials Science and Engineering: B 113 (2004) 60–66.

[9] J.J. Urban, W.S. Yun, Q. Gu, H. Park, Synthesis of single-crystalline perovskite nanorods composed of barium titanate and strontium titanate, Journal of the American Ceramic Society 124 (2002) 1186–1187.

[10] R.K. Roeder, E.B. Slamovich, Stoichiometry control and phase selection in hydrothermally derived $Ba_xSr_{1-x}TiO_3$ powders, Journal of the American Ceramic Society 82 (1999) 1665–1675.

[11] M.I. Diaz-Guemes, T. Gonzalez Carrenõ, C.J. Serna, J.M. Palacios, Mechanism of formation of $MTiO_3$ (M=Sr or Ba) by the gel method, Journal of Materials Science 24 (1989) 1011–1014.

[12] V.R. Calderone, A. Testino, M.T. Buscaglia, M. Bassoli, C. Bottino, M. Viviani, V. Buscaglia, P. Nanni, Size and shape control of $SrTiO_3$ particles grown by epitaxial self-assembly, Chemistry of Materials 18 (2006) 1627–1633.

[13] F.A. Rabuffetti, H.S. Kim, J.A. Enterkin, Y. Wang, C.H. Lanier, L.D. Marks, K.R. Poeppelmeier, P.C. Stair, Synthesis-dependent first-order Raman scattering in $SrTiO_3$ nanocubes at room temperature, Chemistry of Materials 20 (2008) 5628–5635.

[14] S. Fuentes, R.A. Zarate, E. Chavez, P. Muñoz, D. Díaz-Droguett, P. Leyton, Preparation of $SrTiO_3$ nanomaterial by a sol–gel-hydrothermal method, Journal of Materials Science 45 (2010) 1448–1452.

[15] X. Wei, G. Xu, Z. Ren, C. Xu, G. Shen, G. Han, PVA-assisted hydrothermal synthesis of $SrTiO_3$ nanoparticles with enhanced photocatalytic activity for degradation of RhB, Journal of the American Chemical Society 91 (2008) 3795–3799.

[16] C.M. Brooks, L.F. Kourkoutis, T. Heeg, J. Schubert, D.A. Muller, D.G. Schlom, Growth of homoepitaxial $SrTiO_3$ thin films by molecular-beam epitaxy, Applied Physics Letters 94 (2009) 162905.

[17] K. Kiss, J. Magder, M.S. Vukasovich, R.J. Lockhart, Ferroelectrics of ultrafine particle size: I, synthesis of titanate powders of ultrafine particle size, Journal of the American Chemical Society 59 (1966) 291–295.

[18] A. Beran, E. Libowitzky, T. Arambruster, A single-crystal infrared spectroscopic and X-ray diffraction study on untwinned san benito perovskite containing OH groups, The Canadian Mineralogist 34 (1996) 803–809.

[19] W.M. Haynes, in: Handbook of Chemistry and Physics, ninety-second ed., CRC press, Taylor & Francis Group, London, 2011.

[20] S. Doeuff, M Henry, S. Sanchez, J. Livage, Hydrolysis of titanium alkoxides: modification of the molecular precursor by acetic acid, Journal of Non-Crystalline Solids 89 (1987) 206–216.

[21] C.H. Perry, B.N. Khanna, G. Rupprecht G, Infrared studies of Perovskites, Physical Review A 135 (1964) 408–412.

[22] M.D. Judd, M.I. Pope, Energy of activation for the decomposition of the alkaline-earth carbonates from thermogravimetric data, Journal of Thermal Analysis and Calorimetry 4 (1972) 31–38.

[23] J. Poth, R. Haberkorn, H.P. Beck, Combustion-synthesis of $SrTiO_3$, Part II: Sintering behaviour and surface characterization, Journal of the European Ceramic Society 20 (2000) 715–723.

[24] D.Y. Kang, J. Zang, E.R. Wright, A.L. McCanna, C.W. Jones, S. Nair, Dehydration, dehydroxylation, and rehydroxylation of single-walled aluminosilicate nanotubes, ACS Nano 4 (2010) 4897–4907.

[25] R. Vivekanandan, S. Philip, T.R.N. Kutty, Hydrothermal preparation of $Ba(Ti,Zr)O_3$ fine powders, Materials Research Bulletin 22 (1987) 99–108.

[26] S. Wada, T. Suzuki, N. Tatsuo, The effect of the particle sizes and the correlational sizes of dipoles introduced by the lattice defects on the crystal structure of barium titanate fine particles, Japanese Journal of Applied Physics 34 (1995) 5368–5379.

[27] D. Hennings, S. Schreinemacher, Characterization of hydrothermal barium titanate, Journal of the European Ceramic Society 9 (1992) 41–46.

[28] T. Noma, S. Wada, M. Yano, T. Suzuki, Analysis of lattice vibration in fine particles of barium titanate single crystals including lattice hydroxyl group, Journal of Applied Physics 80 (1996) 5223–5233.

[29] E.W. Shi, C.T. Xia, W.Z. Zhong, B.G. Wang, C.D. Feng, Crystallographic properties of hydrothermal barium titanate crystallites, Journal of the American Ceramic Society 80 (1997) 1567–1572.

[30] I.J. Clark, T. Takeuchi, N. Ohtori, D.C. Sinclair, Hydrothermal synthesis and characterisation of $BaTiO_3$ fine powders: precursors, polymorphism and properties, Journal of Materials Chemistry 9 (1999) 83–91.
[31] W.G. Nilsen, J.G. Skinner, Raman spectrum of strontium titanate, Journal of Chemical Physics 48 (1968) 2240–2248.
[32] J. Petzelta, I. Gregoraa, I. Rychetskýa, T. Ostapchuka, S. Kambaa, P. Vaněka, Y. Yuzyukb, A. Almeidab, M.R. Chavezb, B. Gorshunovc, M. Dresselc, S. Hoffmann-Eifertd, R. Waserd, Polar grain boundaries in undoped $SrTiO_3$ ceramics, Journal of the European Ceramic Society 21 (2001) 2681–2686.
[33] S. Banerjee, D.I. Kim, R.D. Robinson, I.P. Herman, Y. Mao, S.S. Wong, Observation of Fano asymmetry in Raman spectra of $SrTiO_3$ and $Ca_xSr_{1-x}TiO_3$ perovskite nanocubes, Applied Physics Letters 89 (2006) 223130.
[34] A.A. Sirenko, I.A. Akimov, J.R. Fox, A.M. Clark, H.C. Li, W. Si, X.X. Xi, Observation of the first-order Raman scattering in $SrTiO_3$ thin films, Physical Review Letters 82 (1999) 4500–4503.
[35] Y. Wang, H. Xu, X. Wang, X. Zhang, H. Jia, L. Zhang, J. Qiu, A general approach to porous crystalline TiO_2, $SrTiO_3$, and $BaTiO_3$ spheres, The Journal of Physical Chemistry B 110 (2006) 13835–13840.
[36] C.-F. Kao, W.-D. Yang, Preparation and electrical properties of fine strontium titanate powder from titanium alkoxide in a strong alkaline solution, Materials Science and Engineering: B 38 (1996) 127–137.
[37] P. Balaya, M. Ahrens, L. Kienle, J. Maier, B. Rahmati, S. Bo Lee, W. Sigle, A. Pashkin, C. Kuntscher, M. Dressel, Synthesis and characterization of nanocrystalline $SrTiO_3$, Journal of the American Ceramic Society 89 (2006) 2804–2811.